RIS-Assisted Full-Duplex Integrated Sensing and Communication

Quang Nhat Le, *Graduate Student Member, IEEE*, Van-Dinh Nguyen, *Member, IEEE*, Octavia A. Dobre, *Fellow, IEEE*, and Hyundong Shin, *Fellow, IEEE*

***Abstract*—In this letter, we explore the application of reconfigurable intelligent surface (RIS) in the integrated sensing and communication network, where a full-duplex multi-antenna base station (BS) concurrently detects a target and communicates with a user equipment (UE). Our objective is to maximize the UE's transmission rate by jointly optimizing the BS's transmit beamforming, UE's transmit power, and RIS's phase shifts, while satisfying the condition on the minimum required sensing power. We develop a block coordinate ascend-based iterative algorithm to solve the formulated problem, which guarantees the convergence to at least a local optimum. Numerical results show the efficiency of the proposed solution as well as the trade-off between the UE's transmission rate and the required sensing power, along with the efficiency of employing RIS.**

***Index Terms*—Full-duplex (FD), integrated sensing and communication (ISAC), reconfigurable intelligent surface (RIS).**

I. Introduction

SENSING is considered an important task of the next-generation cellular networks [1]. Many emerging mobile applications, such as smart manufacturing and industrial Internet-of-Things, not only need high-rate transmission with low latency and high reliability, but also require location information with high accuracy. In order to offer better performance and efficiently utilize spectrum, energy and hardware resources, integrating sensing and communication functions into a single network has become a favorable approach. By jointly optimizing wireless resources, waveform and signal processing flow, a significant performance gain can be achieved in integrated sensing and communication (ISAC) networks [2].

In addition to the ISAC technology, the reconfigurable intelligent surface (RIS) has also received significant attention from both academia and industry [3]. By fine-tuning the phase shift matrix, RIS is able to concurrently modify communication and sensing channels, which is beneficial for ISAC networks [4], [5]. Specifically, RIS can be used to mitigate the interference between the radar and communication systems [6], [7].

Incorporating full-duplex (FD) radio into RIS-ISAC networks can provide great benefits owing to its potential to double the spectral efficiency by enabling transceivers to concurrently transmit and receive data in the same frequency band [4], [8]. In [8], RIS was leveraged to enhance the performance of localization and information retrieval for the FD-ISAC system, in which a FD-base station (BS) simultaneously communicates and senses the position of user equipment (UE).

To reap all the above benefits, in this letter we study the joint active and passive beamforming (BF) design for an RIS-assisted ISAC system, where an FD multi-antenna BS simultaneously communicates with a single antenna UE and detects a target. The BS's transmit beamforming, UE's transmit power, and RIS's reflection coefficients are jointly optimized to maximize the UE's transmission rate subject to the minimum sensing power constraint, transmit power budgets of BS and UE, and unit modulus property of the reflecting elements. The ensuing problem is strongly non-convex and the strong coupling between variables makes it NP-hard. To solve this problem more effectively, we adopt a block coordinate ascend (BCA) algorithm to transform it into two tractable subproblems and develop newly approximated functions to solve them in an iterative fashion. The proposed solution is compared with the maximum ratio transmission (MRT) case, which serves as a benchmark. Simulation results show the notable performance gain achieved with the assistance of RIS, the trade-off between the UE's transmission rate and the required sensing power, and the enhanced performance of the proposed solution compared to the MRT.

II. System Model and Problem Formulation

A. System Model

We consider an RIS-ISAC system, as depicted in Fig. 1, which consists of a dual-functional radar communication (DRC)-BS equipped with M_t transmit antennas and M_r receive antennas; a single-antenna user; an RIS composed of the set $\mathcal{K} \triangleq \{1, 2, \ldots, K\}$ of K elements; and a sensing target. It is supposed that the BS and UE have the knowledge of the location of the RIS [9]. The UE's location can be either obtained by global positioning system or estimated by uplink signals [9]. Let us denote by $\mathbf{f} \in \mathbb{C}^{M_r \times 1}$, $\mathbf{h} \in \mathbb{C}^{1 \times K}$, $\mathbf{A}_u \in \mathbb{C}^{M_r \times K}$, $\mathbf{b}_d \in \mathbb{C}^{M_t \times 1}$, $\mathbf{A}_d \in \mathbb{C}^{M_t \times K}$, $\mathbf{d}_d \in \mathbb{C}^{K \times 1}$, $\mathbf{b}_u \in \mathbb{C}^{M_r \times 1}$, $\mathbf{d}_u \in \mathbb{C}^{K \times 1}$, and $\mathbf{H}_{\mathrm{SI}} \in \mathbb{C}^{M_r \times M_t}$ the channels (matrix/vector) from UE to DRC-BS, from UE to RIS, from

Manuscript received 23 April 2023; revised 19 May 2023; accepted 2 June 2023. Date of publication 12 June 2023; date of current version 9 October 2023. The work of Quang Nhat Le and Octavia A. Dobre was supported by the Natural Sciences and Engineering Research Council of Canada (NSERC) through its Discovery Program. The work of Van-Dinh Nguyen was supported by the VinUniversity Seed Grant Program. The work of Hyundong Shin was supported by the National Research Foundation of Korea (NRF) Grant funded by the Korea Government (MSIT) under Grant 2019R1A2C2007037 and Grant 2022R1A4A3033401. The associate editor coordinating the review of this article and approving it for publication was Y. Zhu. *(Corresponding authors: Octavia A. Dobre; Hyundong Shin.)*

Quang Nhat Le and Octavia A. Dobre are with the Department of Electrical and Computer Engineering, Memorial University, St. John's, NL A1B 3X9, Canada (e-mail: qnle@mun.ca; odobre@mun.ca).

Van-Dinh Nguyen is with the College of Engineering and Computer Science, VinUniversity, 100000 Hanoi, Vietnam (e-mail: dinh.nv2@vinuni.edu.vn).

Hyundong Shin is with the Department of Electronic Engineering, Kyung Hee University, Yongin 17104, South Korea (e-mail: hshin@khu.ac.kr).

Digital Object Identifier 10.1109/LWC.2023.3285391

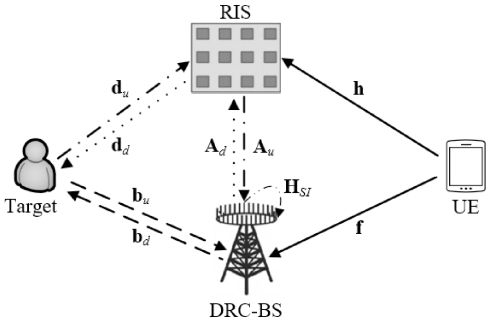

Fig. 1. The RIS-ISAC system.

RIS to DRC-BS, from DRC-BS to target, from DRC-BS to RIS, from RIS to target, from target to DRC-BS, from target to RIS, and the self-interference link of DRC-BS, respectively. The phase shift matrix of RIS is represented by $\mathbf{\Phi} \in \mathbb{C}^{K\times K}$. We also denote by $\xi \in \mathbb{R}^+$ and $\boldsymbol{v} \in \mathbb{C}^{M_t\times 1}$ the transmit power of the UE and the transmit beamforming of DRC-BS, respectively. The signal received at the DRC-BS can be expressed as

$$\begin{aligned}\mathbf{y}(\boldsymbol{\theta},\xi,\boldsymbol{v}) &= \left(\mathbf{f}+\mathbf{A}_u\mathbf{\Phi}\mathbf{h}^H\right)\sqrt{\xi}x_c+\mathbf{H}_{\mathrm{SI}}\boldsymbol{v}x_s\\ &\quad+(\mathbf{b}_u+\mathbf{A}_u\mathbf{\Phi}\mathbf{d}_u)\left(\mathbf{b}_d^H+\mathbf{d}_d^H\mathbf{\Phi}\mathbf{A}_d^H\right)\boldsymbol{v}x_s+\mathbf{n}_n\\ &= (\mathbf{f}+\mathbf{A}_u\mathrm{diag}(\mathbf{h})\boldsymbol{\theta})\sqrt{\xi}x_c\\ &\quad+(\mathbf{b}_u+\mathbf{A}_u\mathrm{diag}(\mathbf{d}_u)\boldsymbol{\theta})\left(\mathbf{b}_d^H+\boldsymbol{\theta}^T\mathrm{diag}(\mathbf{d}_d)\mathbf{A}_d^H\right)\boldsymbol{v}x_s\\ &\quad+\mathbf{H}_{\mathrm{SI}}\boldsymbol{v}x_s+\mathbf{n}_n,\end{aligned} \tag{1}$$

where x_c and x_s are the communication and sensing signals, respectively, and $\mathbf{n}_n \sim \mathcal{CN}(0,\sigma^2)$ is the additive white Gaussian noise (AWGN) with zero-mean and variance σ^2. To simplify the mathematical notations, we denote $\mathbf{\Phi} \triangleq \mathrm{diag}(e^{j\psi_1},e^{j\psi_2},\ldots,e^{j\psi_K}) = \mathrm{diag}(\theta_1,\theta_2,\ldots,\theta_K)$, $\boldsymbol{\theta}=[\theta_1,\theta_2,\ldots,\theta_K]^T$, $\hat{\mathbf{f}}(\boldsymbol{\theta})=\mathbf{f}+\mathbf{A}_u\mathrm{diag}(\mathbf{h})\boldsymbol{\theta}$, and $\hat{\mathbf{b}}^H(\boldsymbol{\theta}) = (\mathbf{b}_u+\mathbf{A}_u\mathrm{diag}(\mathbf{d}_u)\boldsymbol{\theta})(\mathbf{b}_d^H+\boldsymbol{\theta}^T\mathrm{diag}(\mathbf{d}_d)\mathbf{A}_d^H) = \hat{\mathbf{b}}_u(\boldsymbol{\theta})\hat{\mathbf{b}}_d^H(\boldsymbol{\theta})$. As a result, we can rewrite (1) as $\mathbf{y}(\boldsymbol{\theta},\xi,\boldsymbol{v}) = \hat{\mathbf{f}}(\boldsymbol{\theta})\sqrt{\xi}x_c + \hat{\mathbf{b}}^H(\boldsymbol{\theta})\boldsymbol{v}x_s + \mathbf{H}_{\mathrm{SI}}\boldsymbol{v}x_s + \mathbf{n}_n$. The signal-to-interference-plus-noise ratio (SINR) of UE at DRC-BS is given as

$$\gamma_c(\boldsymbol{\theta},\xi,\boldsymbol{v}) = \frac{\left\|\hat{\mathbf{f}}(\boldsymbol{\theta})\right\|^2\xi}{\left\|\hat{\mathbf{b}}^H(\boldsymbol{\theta})\boldsymbol{v}\right\|^2+\left\|\mathbf{H}_{\mathrm{SI}}\boldsymbol{v}\right\|^2+\sigma^2}. \tag{2}$$

B. Problem Formulation

We are interested in maximizing the UE's transmission rate subject to the required sensing power at the DRC-BS by jointly optimizing the involved variables $(\xi,\boldsymbol{v},\boldsymbol{\theta})$. The optimization problem is formulated as

$$\max_{\xi,\boldsymbol{v},\boldsymbol{\theta}} \ \mathcal{R}(\xi,\boldsymbol{v},\boldsymbol{\theta}) \triangleq \ln(1+\gamma_c(\boldsymbol{\theta},\xi,\boldsymbol{v})) \tag{3a}$$

$$\text{s.t.} \ \ \xi \le P_{UE}^{\max} \tag{3b}$$

$$\|\boldsymbol{v}\|^2 \le P_{BS}^{\max} \tag{3c}$$

$$\left\|\hat{\mathbf{b}}^H(\boldsymbol{\theta})\boldsymbol{v}\right\|^2 \ge P_{\mathrm{sense}} \tag{3d}$$

$$|\theta_k| = 1, \forall k \in \mathcal{K}, \tag{3e}$$

where (3b) and (3c) indicate the power constraints at the UE and DRC-BS with the maximum transmit powers $P_{UE}^{\max}$ and $P_{BS}^{\max}$, respectively. Constraint (3d) describes the required sensing power at the DRC-BS with P_{sense} being the minimum sensing power. Finally, (3e) presents the RIS phase shift constraint. From (3d), the target's location can be estimated by the BS as long as the received signal strength of the echo probing signal is larger than or equal to the required sensing power.

III. Proposed Solution

We adopt the BCA approach and decouple (3) into two subproblems corresponding to $(\xi,\boldsymbol{v})$ and $\boldsymbol{\theta}$, each of which will be solved by the inner approximation (IA) method [10]. At iteration η, let $(\xi^{(\eta)},\boldsymbol{v}^{(\eta)},\boldsymbol{\theta}^{(\eta)})$ be the feasible point for (3) that is found from the $(\eta-1)$-th round. By BCA, we solve problem (3) to obtain the optimal solutions $(\xi^\star,\boldsymbol{v}^\star)$ for given $\boldsymbol{\theta}^{(\eta)}$, and then update $(\xi^{(\eta+1)} := \xi^\star, \boldsymbol{v}^{(\eta+1)} := \boldsymbol{v}^\star)$ to solve (3) with respect to $\boldsymbol{\theta}$.

A. Transmit Power and Beamforming Iteration

For a given $\boldsymbol{\theta}^{(\eta)}$, (3) is rewritten at iteration $\eta+1$ as:

$$\max_{\xi,\boldsymbol{v}} \ \mathcal{R}(\xi,\boldsymbol{v},\boldsymbol{\theta}^{(\eta)}) \triangleq \ln\left(1+\frac{\left\|\hat{\mathbf{f}}(\boldsymbol{\theta}^{(\eta)})\right\|^2\xi}{\left\|\hat{\mathbf{b}}^H(\boldsymbol{\theta}^{(\eta)})\boldsymbol{v}\right\|^2+\left\|\mathbf{H}_{\mathrm{SI}}\boldsymbol{v}\right\|^2+\sigma^2}\right) \tag{4a}$$

$$\text{s.t.} \ \ \xi \le P_{UE}^{\max} \tag{4b}$$

$$\|\boldsymbol{v}\|^2 \le P_{BS}^{\max} \tag{4c}$$

$$\left\|\hat{\mathbf{b}}^H(\boldsymbol{\theta}^{(\eta)})\boldsymbol{v}\right\|^2 \ge P_{\mathrm{sense}}, \tag{4d}$$

where the objective (4a) is non-concave while (4d) is the non-convex constraint. The concave lower bound of (4a) can be found as [11, eq. (62)]:

$$\begin{aligned}&\ln\left(1+\frac{\left\|\hat{\mathbf{f}}(\boldsymbol{\theta}^{(\eta)})\right\|^2\xi}{\left\|\hat{\mathbf{b}}^H(\boldsymbol{\theta}^{(\eta)})\boldsymbol{v}\right\|^2+\left\|\mathbf{H}_{\mathrm{SI}}\boldsymbol{v}\right\|^2+\sigma^2}\right)\\ &\ge \ln\left(1+\frac{\left\|\hat{\mathbf{f}}(\boldsymbol{\theta}^{(\eta)})\right\|^2\xi^{(\eta)}}{\left\|\hat{\mathbf{b}}^H(\boldsymbol{\theta}^{(\eta)})\boldsymbol{v}^{(\eta)}\right\|^2+\left\|\mathbf{H}_{\mathrm{SI}}\boldsymbol{v}^{(\eta)}\right\|^2+\sigma^2}\right)\\ &\quad+\frac{\left\|\hat{\mathbf{f}}(\boldsymbol{\theta}^{(\eta)})\right\|^2\xi^{(\eta)}}{\left\|\hat{\mathbf{b}}^H(\boldsymbol{\theta}^{(\eta)})\boldsymbol{v}^{(\eta)}\right\|^2+\left\|\mathbf{H}_{\mathrm{SI}}\boldsymbol{v}^{(\eta)}\right\|^2+\sigma^2+\left\|\hat{\mathbf{f}}(\boldsymbol{\theta}^{(\eta)})\right\|^2\xi^{(\eta)}}\\ &\quad\times\left(2-\frac{\xi^{(\eta)}}{\xi}-\frac{\left\|\hat{\mathbf{b}}^H(\boldsymbol{\theta}^{(\eta)})\boldsymbol{v}\right\|^2+\left\|\mathbf{H}_{\mathrm{SI}}\boldsymbol{v}\right\|^2+\sigma^2}{\left\|\hat{\mathbf{b}}^H(\boldsymbol{\theta}^{(\eta)})\boldsymbol{v}^{(\eta)}\right\|^2+\left\|\mathbf{H}_{\mathrm{SI}}\boldsymbol{v}^{(\eta)}\right\|^2+\sigma^2}\right)\\ &:= \mathcal{R}^{(\eta)}(\xi,\boldsymbol{v}|\boldsymbol{\theta}^{(\eta)}).\end{aligned} \tag{5}$$

Next, the left-hand side (LHS) of (4d) is a quadratic function which can be innerly approximated as

$$2\Re\{(\boldsymbol{v}^{(\eta)})^H\hat{\mathbf{b}}(\boldsymbol{\theta}^{(\eta)})\hat{\mathbf{b}}^H(\boldsymbol{\theta}^{(\eta)})\boldsymbol{v}\}-\left\|\hat{\mathbf{b}}^H(\boldsymbol{\theta}^{(\eta)})\boldsymbol{v}^{(\eta)}\right\|^2 \ge P_{\mathrm{sense}}. \tag{6}$$

In summary, the approximate convex program of (4) solved at iteration $\eta+1$ is expressed by

$$\max_{\xi,\boldsymbol{v}} \ \mathcal{R}^{(\eta)}(\xi,\boldsymbol{v}|\boldsymbol{\theta}^{(\eta)}) \tag{7a}$$

$$\text{s.t.} \quad \text{(4b), (4c), (6).} \tag{7b}$$

B. Phase Shift Iteration

For given $(\xi^{(\eta+1)},\boldsymbol{v}^{(\eta+1)})$, (3) is rewritten at iteration $\eta+1$ as:

$$\max_{\boldsymbol{\theta}} \ \mathcal{R}(\xi^{(\eta+1)}, \boldsymbol{v}^{(\eta+1)}, \boldsymbol{\theta}) \triangleq \ln\left(1+\frac{\left\|\hat{\mathbf{f}}(\boldsymbol{\theta})\right\|^2\xi^{(\eta+1)}}{\left\|\hat{\mathbf{b}}^H(\boldsymbol{\theta})\boldsymbol{v}^{(\eta+1)}\right\|^2+\left\|\mathbf{H}_{\mathrm{SI}}\boldsymbol{v}^{(\eta+1)}\right\|^2+\sigma^2}\right) \quad (8a)$$

$$\text{s.t.} \ \left\|\hat{\mathbf{b}}^H(\boldsymbol{\theta})\boldsymbol{v}^{(\eta+1)}\right\|^2 \geq P_{\mathrm{sense}} \quad (8b)$$

$$|\theta_k| = 1, \forall k \in \mathcal{K}, \quad (8c)$$

where the objective (8a) is non-concave, while constraints (8b) and (8c) are non-convex. According to the Cauchy-Schwarz inequality, the first term in the denominator of (8a) can be upper bounded as

$$\begin{aligned}\left\|\hat{\mathbf{b}}^H(\boldsymbol{\theta})\boldsymbol{v}^{(\eta+1)}\right\|^2 &= \left\|\hat{\mathbf{b}}_u(\boldsymbol{\theta})\hat{\mathbf{b}}_d^H(\boldsymbol{\theta})\boldsymbol{v}^{(\eta+1)}\right\|^2 \\ &\leq \left\|\hat{\mathbf{b}}_u(\boldsymbol{\theta})\right\|^2\left\|\hat{\mathbf{b}}_d^H(\boldsymbol{\theta})\boldsymbol{v}^{(\eta+1)}\right\|^2 \\ &\leq t\zeta, \end{aligned} \quad (9)$$

where $t \in \mathbb{R}^+$ and $\zeta \in \mathbb{R}^+$ are newly introduced optimization variables, satisfying $\|\hat{\mathbf{b}}_u(\boldsymbol{\theta})\|^2 \leq t$ and $\|\hat{\mathbf{b}}_d^H(\boldsymbol{\theta})\boldsymbol{v}^{(\eta+1)}\|^2 \leq \zeta$. The product $t\zeta$ is convexified as $t\zeta \leq \frac{t^{(\eta)}\zeta^2}{2\zeta^{(\eta)}} + \frac{\zeta^{(\eta)}t^2}{2t^{(\eta)}}$. Accordingly, the concave lower bound of (8a) is

$$\begin{aligned}&\ln\left(1+\frac{\left\|\hat{\mathbf{f}}(\boldsymbol{\theta})\right\|^2\xi^{(\eta+1)}}{t\zeta+\left\|\mathbf{H}_{\mathrm{SI}}\boldsymbol{v}^{(\eta+1)}\right\|^2+\sigma^2}\right) \\ &\geq \ln\left(1+\frac{\left\|\hat{\mathbf{f}}(\boldsymbol{\theta}^{(\eta)})\right\|^2\xi^{(\eta+1)}}{t^{(\eta)}\zeta^{(\eta)}+\left\|\mathbf{H}_{\mathrm{SI}}\boldsymbol{v}^{(\eta+1)}\right\|^2+\sigma^2}\right) \\ &+\frac{\left\|\hat{\mathbf{f}}(\boldsymbol{\theta}^{(\eta)})\right\|^2\xi^{(\eta+1)}}{t^{(\eta)}\zeta^{(\eta)}+\left\|\mathbf{H}_{\mathrm{SI}}\boldsymbol{v}^{(\eta+1)}\right\|^2+\sigma^2+\left\|\hat{\mathbf{f}}(\boldsymbol{\theta}^{(\eta)})\right\|^2\xi^{(\eta+1)}} \\ &\times\left(2-\frac{\left\|\hat{\mathbf{f}}(\boldsymbol{\theta}^{(\eta)})\right\|^2}{\left\|\hat{\mathbf{f}}(\boldsymbol{\theta})\right\|^2}-\frac{\frac{t^{(\eta)}\zeta^2}{2\zeta^{(\eta)}}+\frac{\zeta^{(\eta)}t^2}{2t^{(\eta)}}+\left\|\mathbf{H}_{\mathrm{SI}}\boldsymbol{v}^{(\eta+1)}\right\|^2+\sigma^2}{t^{(\eta)}\zeta^{(\eta)}+\left\|\mathbf{H}_{\mathrm{SI}}\boldsymbol{v}^{(\eta+1)}\right\|^2+\sigma^2}\right) \\ &\triangleq \mathcal{R}^{(\eta)}(\boldsymbol{\theta}|\xi^{(\eta+1)}, \boldsymbol{v}^{(\eta+1)}). \end{aligned} \quad (10)$$

To convexify (8b), we first approximate its LHS as

$$\left\|\hat{\mathbf{b}}^H(\boldsymbol{\theta})\boldsymbol{v}^{(\eta+1)}\right\|^2 \geq 2\Re\left\{\left(\hat{\mathbf{b}}^H(\boldsymbol{\theta}^{(\eta)})\boldsymbol{v}^{(\eta+1)}\right)^H\hat{\mathbf{b}}^H(\boldsymbol{\theta})\boldsymbol{v}^{(\eta+1)}\right\} - \left\|\hat{\mathbf{b}}^H(\boldsymbol{\theta}^{(\eta)})\boldsymbol{v}^{(\eta+1)}\right\|^2. \quad (11)$$

Then, the first term of the right-hand side of (11) is further rewritten as

$$\begin{aligned}&2\Re\left\{\left(\hat{\mathbf{b}}^H(\boldsymbol{\theta}^{(\eta)})\boldsymbol{v}^{(\eta+1)}\right)^H\hat{\mathbf{b}}^H(\boldsymbol{\theta})\boldsymbol{v}^{(\eta+1)}\right\} \\ &= 2\Re\left\{\left(\hat{\mathbf{b}}^H(\boldsymbol{\theta}^{(\eta)})\boldsymbol{v}^{(\eta+1)}\right)^H\mathbf{b}_u\mathbf{b}_d^H\boldsymbol{v}^{(\eta+1)}\right\} \\ &+2\Re\left\{\left(\hat{\mathbf{b}}^H(\boldsymbol{\theta}^{(\eta)})\boldsymbol{v}^{(\eta+1)}\right)^H\mathbf{b}_u\boldsymbol{\theta}^T\mathrm{diag}(\mathbf{d}_d)\mathbf{A}_d^H\boldsymbol{v}^{(\eta+1)}\right\} \\ &+2\Re\left\{\left(\hat{\mathbf{b}}^H(\boldsymbol{\theta}^{(\eta)})\boldsymbol{v}^{(\eta+1)}\right)^H\mathbf{A}_u\mathrm{diag}(\mathbf{d}_u)\boldsymbol{\theta}\mathbf{b}_d^H\boldsymbol{v}^{(\eta+1)}\right\} \\ &+2\Re\left\{\left(\hat{\mathbf{b}}^H(\boldsymbol{\theta}^{(\eta)})\boldsymbol{v}^{(\eta+1)}\right)^H\mathbf{A}_u\mathrm{diag}(\mathbf{d}_u)\boldsymbol{\theta}\boldsymbol{\theta}^T\mathrm{diag}(\mathbf{d}_d)\mathbf{A}_d^H\boldsymbol{v}^{(\eta+1)}\right\} \\ &\triangleq \mathcal{X}^{(\eta)}(\boldsymbol{\theta}|\boldsymbol{v}^{(\eta+1)}) \\ &+2\Re\left\{\boldsymbol{\theta}^T\mathrm{diag}(\mathbf{d}_d)\mathbf{A}_d^H\boldsymbol{v}^{(\eta+1)}\left(\hat{\mathbf{b}}^H(\boldsymbol{\theta}^{(\eta)})\boldsymbol{v}^{(\eta+1)}\right)^H\mathbf{A}_u\mathrm{diag}(\mathbf{d}_u)\boldsymbol{\theta}\right\} \\ &= \mathcal{X}^{(\eta)}(\boldsymbol{\theta}|\boldsymbol{v}^{(\eta+1)}) + 2\Re\{\boldsymbol{\theta}^T\boldsymbol{\mathcal{Y}}\boldsymbol{\theta}\}, \end{aligned} \quad (12)$$

where $\boldsymbol{\mathcal{Y}} \triangleq \mathrm{diag}(\mathbf{d}_d)\mathbf{A}_d^H\boldsymbol{v}^{(\eta+1)}(\hat{\mathbf{b}}^H(\boldsymbol{\theta}^{(\eta)})\boldsymbol{v}^{(\eta+1)})^H\mathbf{A}_u\mathrm{diag}(\mathbf{d}_u)$. The last term of (12) is convexified as

$$2\Re\left\{\boldsymbol{\theta}^T\boldsymbol{\mathcal{Y}}\boldsymbol{\theta}\right\} \geq 2\Re\left\{(\boldsymbol{\theta}^{(\eta)})^T\boldsymbol{\mathcal{Y}}\boldsymbol{\theta} + \boldsymbol{\theta}^T\boldsymbol{\mathcal{Y}}\boldsymbol{\theta}^{(\eta)} - (\boldsymbol{\theta}^{(\eta)})^T\boldsymbol{\mathcal{Y}}\boldsymbol{\theta}^{(\eta)}\right\}. \quad (13)$$

From (11), (12) and (13), constraint (8b) is innerly approximated as follows:

$$\mathcal{X}^{(\eta)}(\boldsymbol{\theta}|\boldsymbol{v}^{(\eta+1)}) + 2\Re\left\{(\boldsymbol{\theta}^{(\eta)})^T\boldsymbol{\mathcal{Y}}\boldsymbol{\theta} + \boldsymbol{\theta}^T\boldsymbol{\mathcal{Y}}\boldsymbol{\theta}^{(\eta)} - (\boldsymbol{\theta}^{(\eta)})^T\boldsymbol{\mathcal{Y}}\boldsymbol{\theta}^{(\eta)}\right\} - \left\|\hat{\mathbf{b}}^H(\boldsymbol{\theta}^{(\eta)})\boldsymbol{v}^{(\eta+1)}\right\|^2 \geq P_{\mathrm{sense}}. \quad (14)$$

Further, the unit-modulus constraint (8c) is relaxed by the following convex constraint:

$$|\theta_k|^2 \leq 1, \forall k \in \mathcal{K}, \quad (15)$$

which means that $\sum_{k\in\mathcal{K}}|\theta_k|^2 - K \leq 0$. To guarantee that constraint (8c) is satisfied at optimum, we establish the following theorem.

Theorem 1: The following penalized optimization problem is used to ensure the optimality of (8):

$$\max_{\boldsymbol{\theta}} \ \mathcal{R}(\xi^{(\eta+1)}, \boldsymbol{v}^{(\eta+1)}, \boldsymbol{\theta}) + \varrho\Big(\sum_{k\in\mathcal{K}}|\theta_k|^2 - K\Big) \quad (16a)$$

$$\text{s.t.} \quad (8b), \ (15), \quad (16b)$$

where $\varrho > 0$ denotes a penalty parameter such that the objective and penalty terms become comparable.

Proof: Owing to constraint (15), the penalty term $\sum_{k\in\mathcal{K}}|\theta_k|^2 - K$ is always negative. A positive value of ϱ enables the uncertainties of the unit-modulus constraint to be penalized, which guarantees $\theta_k = 1$ at optimum. If ϱ is sufficiently large, (8) and (16) have the same optimal solution. The steps of a similar proof are found in [12, Appendix C]. ■

Summing up, the approximate convex program of (8) solved at iteration $\eta+1$ is expressed by

$$\max_{\boldsymbol{\theta},t,\zeta} \ \mathcal{R}^{(\eta)}(\xi^{(\eta+1)}, \boldsymbol{v}^{(\eta+1)}, \boldsymbol{\theta}) \triangleq \mathcal{R}^{(\eta)}(\boldsymbol{\theta}|\xi^{(\eta+1)}, \boldsymbol{v}^{(\eta+1)}) + \varrho\Big(\mathcal{P}^{(\eta)}(\boldsymbol{\theta}) - K\Big) \quad (17a)$$

$$\text{s.t.} \ \left\|\hat{\mathbf{b}}_u(\boldsymbol{\theta})\right\|^2 \leq t \quad (17b)$$

$$\left\|\hat{\mathbf{b}}_d^H(\boldsymbol{\theta})\boldsymbol{v}^{(\eta+1)}\right\|^2 \leq \zeta \quad (17c)$$

$$|\theta_k|^2 \leq 1, \forall k \in \mathcal{K} \quad (17d)$$

$$(14), \quad (17e)$$

where $\mathcal{P}^{(\eta)}(\boldsymbol{\theta}) \triangleq \sum_{k\in\mathcal{K}}(2\Re\{(\theta_k^{(\eta)})^*\theta_k\} - |\theta_k^{(\eta)}|^2)$.

Algorithm 1 summarizes the BCA-based algorithm for solving (3).

Complexity and convergence analysis: The computational complexity of solving (7) and (17) is $\mathcal{O}((M_t+1)^2 3^{2.5}+3^{3.5})$ and $\mathcal{O}((K+2)^2(K+3)^{2.5}+(K+3)^{3.5})$ for each iteration, respectively. On the other hand, from the IA principles, it is obvious from (7) that $\mathcal{R}(\xi^{(\eta+1)}, \boldsymbol{v}^{(\eta+1)}, \boldsymbol{\theta}^{(\eta)}) \geq \mathcal{R}^{(\eta)}(\xi^{(\eta+1)}, \boldsymbol{v}^{(\eta+1)}|\boldsymbol{\theta}^{(\eta)}) \geq \mathcal{R}^{(\eta)}(\xi^{(\eta)}, \boldsymbol{v}^{(\eta)}|\boldsymbol{\theta}^{(\eta)}) = \mathcal{R}(\xi^{(\eta)}, \boldsymbol{v}^{(\eta)}, \boldsymbol{\theta}^{(\eta)})$. As in (17), we have $\mathcal{R}(\xi^{(\eta+1)}, \boldsymbol{v}^{(\eta+1)}, \boldsymbol{\theta}^{(\eta+1)}) \geq \mathcal{R}^{(\eta)}(\xi^{(\eta+1)}, \boldsymbol{v}^{(\eta+1)}, \boldsymbol{\theta}^{(\eta+1)}) \geq \mathcal{R}^{(\eta)}(\xi^{(\eta+1)}, \boldsymbol{v}^{(\eta+1)}, \boldsymbol{\theta}^{(\eta)}) = \mathcal{R}(\xi^{(\eta+1)}, \boldsymbol{v}^{(\eta+1)}, \boldsymbol{\theta}^{(\eta)})$. Accordingly, it holds true that $\mathcal{R}(\xi^{(\eta+1)}, \boldsymbol{v}^{(\eta+1)}, \boldsymbol{\theta}^{(\eta+1)}) \geq$

Algorithm 1 Proposed BCA-Based Iterative Algorithm to Solve (3)

Initialization: Set $\eta := 0$. Generate an initial feasible point $(\xi^{(0)}, \boldsymbol{v}^{(0)}, \boldsymbol{\theta}^{(0)}, t^{(0)}, \zeta^{(0)})$;

1: **repeat**
2: Given $\boldsymbol{\theta}^{(\eta)}$, solve (7) to obtain $(\xi^\star, \boldsymbol{v}^\star)$ and update $(\xi^{(\eta+1)}, \boldsymbol{v}^{(\eta+1)}) := (\xi^\star, \boldsymbol{v}^\star)$;
3: Given $(\xi^{(\eta+1)}, \boldsymbol{v}^{(\eta+1)})$, solve (17) to obtain $\boldsymbol{\theta}^\star$ and update $\boldsymbol{\theta}^{(\eta+1)} := \boldsymbol{\theta}^\star$;
4: Set $\eta := \eta + 1$;
5: **until** Convergence
6: **Ouput**: $(\xi^\star, \boldsymbol{v}^\star, \boldsymbol{\theta}^\star)$

$\mathcal{R}(\xi^{(\eta)}, \boldsymbol{v}^{(\eta)}, \boldsymbol{\theta}^{(\eta)})$. Thus, Algorithm 1 yields a sequence $\{(\xi^{(\eta)}, \boldsymbol{v}^{(\eta)}, \boldsymbol{\theta}^{(\eta)})\}$ of points that converges at least to a locally optimal solution [13].

C. Sub-Optimal Design Based on MRT

To reduce the complexity of the active beamforming, we adopt the MRT by $\boldsymbol{v} = \frac{\sqrt{\beta}\mathbf{b}_d}{\|\mathbf{b}_d\|}$, where β is the power level. The MRT-based optimization problem is re-formulated as follows

$$\max_{\xi,\beta,\boldsymbol{\theta}} \ \mathcal{R}(\xi,\beta,\boldsymbol{\theta}) \triangleq \ln\left(1+\frac{\|\hat{\mathbf{f}}(\boldsymbol{\theta})\|^2\xi}{\beta\|\hat{\mathbf{b}}^H(\boldsymbol{\theta})\frac{\mathbf{b}_d}{\|\mathbf{b}_d\|}\|^2+\beta\|\mathbf{H}_{\mathrm{SI}}\frac{\mathbf{b}_d}{\|\mathbf{b}_d\|}\|^2+\sigma^2}\right) \tag{18a}$$

$$\text{s.t.} \quad \xi \le P_{UE}^{\max} \tag{18b}$$

$$\beta \le P_{BS}^{\max} \tag{18c}$$

$$\beta\|\hat{\mathbf{b}}^H(\boldsymbol{\theta})\frac{\mathbf{b}_d}{\|\mathbf{b}_d\|}\|^2 \ge P_{\mathrm{sense}} \tag{18d}$$

$$|\theta_k| = 1, \forall k \in \mathcal{K}. \tag{18e}$$

Based on (5), the convex problem of transmit power and beamforming solved at iteration $\eta+1$ is given by

$$\max_{\xi,\beta} \ \mathcal{R}^{(\eta)}(\xi,\beta|\boldsymbol{\theta}^{(\eta)}) \tag{19a}$$

$$\text{s.t.} \quad \text{(18b), (18c), (18d),} \tag{19b}$$

where

$$\mathcal{R}^{(\eta)}(\xi,\beta|\boldsymbol{\theta}^{(\eta)}) \triangleq \ln\left(1+\frac{\|\hat{\mathbf{f}}(\boldsymbol{\theta}^{(\eta)})\|^2\xi^{(\eta)}}{\beta^{(\eta)}\|\hat{\mathbf{b}}^H(\boldsymbol{\theta}^{(\eta)})\frac{\mathbf{b}_d}{\|\mathbf{b}_d\|}\|^2+\beta^{(\eta)}\|\mathbf{H}_{\mathrm{SI}}\frac{\mathbf{b}_d}{\|\mathbf{b}_d\|}\|^2+\sigma^2}\right) + \frac{\|\hat{\mathbf{f}}(\boldsymbol{\theta}^{(\eta)})\|^2\xi^{(\eta)}}{\beta^{(\eta)}\|\hat{\mathbf{b}}^H(\boldsymbol{\theta}^{(\eta)})\frac{\mathbf{b}_d}{\|\mathbf{b}_d\|}\|^2+\beta^{(\eta)}\|\mathbf{H}_{\mathrm{SI}}\frac{\mathbf{b}_d}{\|\mathbf{b}_d\|}\|^2+\sigma^2+\|\hat{\mathbf{f}}(\boldsymbol{\theta}^{(\eta)})\|^2\xi^{(\eta)}} \times\left(2-\frac{\xi^{(\eta)}}{\xi}-\frac{\beta\|\hat{\mathbf{b}}^H(\boldsymbol{\theta}^{(\eta)})\frac{\mathbf{b}_d}{\|\mathbf{b}_d\|}\|^2+\beta\|\mathbf{H}_{\mathrm{SI}}\frac{\mathbf{b}_d}{\|\mathbf{b}_d\|}\|^2+\sigma^2}{\beta^{(\eta)}\|\hat{\mathbf{b}}^H(\boldsymbol{\theta}^{(\eta)})\frac{\mathbf{b}_d}{\|\mathbf{b}_d\|}\|^2+\beta^{(\eta)}\|\mathbf{H}_{\mathrm{SI}}\frac{\mathbf{b}_d}{\|\mathbf{b}_d\|}\|^2+\sigma^2}\right).$$

Based on (9), (10) and (14), the convex problem of phase shift iteration solved at iteration $\eta+1$ is expressed by

$$\max_{\boldsymbol{\theta},t,\zeta} \ \mathcal{Q}^{(\eta)}(\xi^{(\eta+1)},\beta^{(\eta+1)},\boldsymbol{\theta}) \triangleq \mathcal{Q}^{(\eta)}(\boldsymbol{\theta}|\xi^{(\eta+1)},\beta^{(\eta+1)}) + \varrho\Big(\mathcal{P}^{(\eta)}(\boldsymbol{\theta})-K\Big) \tag{20a}$$

$$\text{s.t.} \quad \|\hat{\mathbf{b}}_u(\boldsymbol{\theta})\|^2 \le t \tag{20b}$$

$$\|\hat{\mathbf{b}}_d^H(\boldsymbol{\theta})\frac{\mathbf{b}_d}{\|\mathbf{b}_d\|}\|^2 \le \zeta \tag{20c}$$

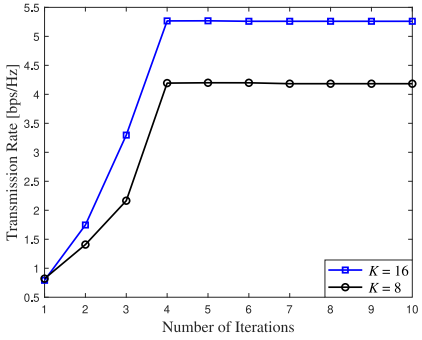

Fig. 2. Convergence rate of Algorithm 1 with different values of K.

$$\beta^{(\eta+1)}2\Re\Big\{(\boldsymbol{\theta}^{(\eta)})^T\boldsymbol{\mathcal{Y}}\boldsymbol{\theta}+\boldsymbol{\theta}^T\boldsymbol{\mathcal{Y}}\boldsymbol{\theta}^{(\eta)}-(\boldsymbol{\theta}^{(\eta)})^T\boldsymbol{\mathcal{Y}}\boldsymbol{\theta}^{(\eta)}\Big\} + \mathcal{X}^{(\eta)}(\boldsymbol{\theta}|\beta^{(\eta+1)}) - \beta^{(\eta+1)}\|\hat{\mathbf{b}}^H(\boldsymbol{\theta}^{(\eta)})\frac{\mathbf{b}_d}{\|\mathbf{b}_d\|}\|^2 \ge P_{\mathrm{sense}} \tag{20d}$$

$$|\theta_k|^2 \le 1, \forall k \in \mathcal{K}, \tag{20e}$$

where

$$\mathcal{Q}^{(\eta)}(\boldsymbol{\theta}|\xi^{(\eta+1)},\beta^{(\eta+1)}) \triangleq \ln\left(1+\frac{\|\hat{\mathbf{f}}(\boldsymbol{\theta}^{(\eta)})\|^2\xi^{(\eta+1)}}{\beta^{(\eta+1)}t^{(\eta)}\zeta^{(\eta)}+\beta^{(\eta+1)}\|\mathbf{H}_{\mathrm{SI}}\frac{\mathbf{b}_d}{\|\mathbf{b}_d\|}\|^2+\sigma^2}\right) + \frac{\|\hat{\mathbf{f}}(\boldsymbol{\theta}^{(\eta)})\|^2\xi^{(\eta+1)}}{\beta^{(\eta+1)}t^{(\eta)}\zeta^{(\eta)}+\beta^{(\eta+1)}\|\mathbf{H}_{\mathrm{SI}}\frac{\mathbf{b}_d}{\|\mathbf{b}_d\|}\|^2+\sigma^2+\|\hat{\mathbf{f}}(\boldsymbol{\theta}^{(\eta)})\|^2\xi^{(\eta+1)}} \times\left(2-\frac{\|\hat{\mathbf{f}}(\boldsymbol{\theta}^{(\eta)})\|^2}{\|\hat{\mathbf{f}}(\boldsymbol{\theta})\|^2}-\frac{\frac{t^{(\eta)}\zeta^2}{2\zeta^{(\eta)}}+\frac{\zeta^{(\eta)}t^2}{2t^{(\eta)}}+\|\mathbf{H}_{\mathrm{SI}}\frac{\mathbf{b}_d}{\|\mathbf{b}_d\|}\|^2+\frac{\sigma^2}{\beta^{(\eta+1)}}}{t^{(\eta)}\zeta^{(\eta)}+\|\mathbf{H}_{\mathrm{SI}}\frac{\mathbf{b}_d}{\|\mathbf{b}_d\|}\|^2+\frac{\sigma^2}{\beta^{(\eta+1)}}}\right),$$

$$\mathcal{X}^{(\eta)}(\boldsymbol{\theta}|\beta^{(\eta+1)}) \triangleq \beta^{(\eta+1)}2\Re\left\{\left(\hat{\mathbf{b}}^H(\boldsymbol{\theta}^{(\eta)})\frac{\mathbf{b}_d}{\|\mathbf{b}_d\|}\right)^H\mathbf{b}_u\mathbf{b}_d^H\frac{\mathbf{b}_d}{\|\mathbf{b}_d\|}\right\} + \beta^{(\eta+1)}2\Re\left\{\left(\hat{\mathbf{b}}^H(\boldsymbol{\theta}^{(\eta)})\frac{\mathbf{b}_d}{\|\mathbf{b}_d\|}\right)^H\mathbf{b}_u\boldsymbol{\theta}^T\mathrm{diag}(\mathbf{d}_d)\mathbf{A}_d^H\frac{\mathbf{b}_d}{\|\mathbf{b}_d\|}\right\} + \beta^{(\eta+1)}2\Re\left\{\left(\hat{\mathbf{b}}^H(\boldsymbol{\theta}^{(\eta)})\frac{\mathbf{b}_d}{\|\mathbf{b}_d\|}\right)^H\mathbf{A}_u\mathrm{diag}(\mathbf{d}_u)\boldsymbol{\theta}\mathbf{b}_d^H\frac{\mathbf{b}_d}{\|\mathbf{b}_d\|}\right\}$$

and $\boldsymbol{\mathcal{Y}} \triangleq \mathrm{diag}(\mathbf{d}_d)\mathbf{A}_d^H\frac{\mathbf{b}_d}{\|\mathbf{b}_d\|}(\hat{\mathbf{b}}^H(\boldsymbol{\theta}^{(\eta)})\frac{\mathbf{b}_d}{\|\mathbf{b}_d\|})^H\mathbf{A}_u\mathrm{diag}(\mathbf{d}_u)$.

The computational complexity of solving (19) and (20) is $\mathcal{O}(2^2 3^{2.5}+3^{3.5})$ and $\mathcal{O}((K+2)^2(K+3)^{2.5}+(K+3)^{3.5})$ for each iteration, respectively.

IV. Numerical Results

We consider a 2-D scenario, in which the BS, target, UE, and RIS are located at (5 m, 0), (5 m, 50 m), (20 m, 10 m), and (10 m, 10 m), respectively. Unless otherwise stated, the bandwidth is 20 MHz, the BS's maximum transmit power is 1 W, and the UE's maximum transmit power is 5 mW. The number of RIS elements K is 8, the noise power σ^2 at the BS is -80 dBm, and the BS is equipped with $M_t = M_r = 5$ antennas. We utilize the distance-dependent path-loss model [14]; the path-loss exponents of the BS-RIS, RIS-target, RIS-UE, BS-target, and BS-UE links are set to 2.5, 2.8, 2.8, 3, and 3, respectively [15], [16]. All simulation results are obtained over an average of 1000 simulation runs.

Fig. 2 presents Algorithm 1's convergence pattern. Apparently, Algorithm 1 needs about 4 iterations to attain the optimal value of

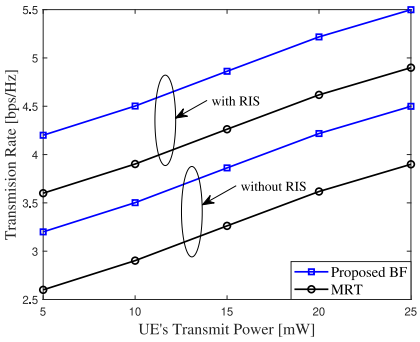

Fig. 3. Transmission rate of the UE versus the UE's transmit power.

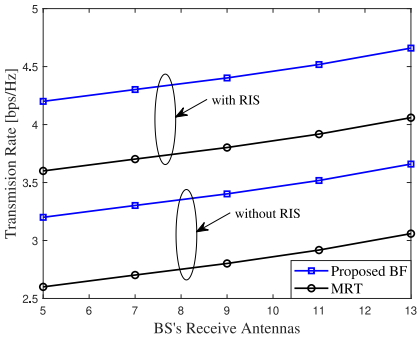

Fig. 4. Transmission rate of the UE versus the BS's receive antennas.

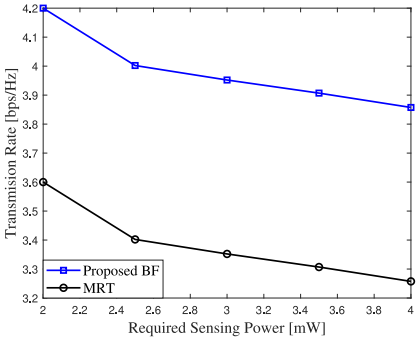

Fig. 5. Transmission rate of the UE versus the required sensing power.

the UE's transmission rate. Also, increasing K leads to enhanced transmission rate of the UE.

Fig. 3 shows the transmission rate versus the UE's transmit power. Not surprisingly, the UE's transmission rate increases with the UE's transmit power. This is because increasing the UE's transmit power results in higher received signal strength at BS. Further, the transmission rate of the proposed transmit BF case is much higher than that of the MRT case regardless if the RIS is utilized or not.

Fig. 4 plots the UE's transmission rate versus the BS's receive antennas. As expected, increasing M_r results in higher transmission rate of the UE. This is attributed to the fact that the higher the value of M_r, the better the received diversity can be obtained, which in turn improves the signal reception quality at BS.

Fig. 5 depicts the trade-off between the UE's transmission rate and the required sensing power. As expected, increasing the required sensing power leads to a decrease in the UE's transmission rate. This is because a higher transmit power at BS is needed to enhance the received sensing signal power, but it conversely degrades the SINR of UE at BS.

V. Conclusion

The transmission rate maximization problem of a FD-ISAC network with the assistance of the RIS was considered in this letter. A non-convex problem was formulated, which involved a joint optimization of the BS's transmit beamforming, UE's transmit power, and RIS's phase shifts. It was solved with a proposed BCA algorithm that relies on the IA framework. Simulation results showed the fast convergence and effectiveness of the algorithm, the trade-off between the UE's transmission rate and the required sensing power, and the advantage of employing RIS. The extensions considering multiple targets or multiple UEs are interesting topics for our future works.

References

[1] X. Li, Y. Cui, J. A. Zhang, F. Liu, D. Zhang, and L. Hanzo, "Integrated human activity sensing and communications," *IEEE Commun. Mag.*, vol. 1, no. 1, pp. 1–8, May 2023.

[2] Z. Wei et al., "Integrated sensing and communication signals towards 5G-A and 6G: A survey," *IEEE Internet Things J.*, early access, Jan. 9, 2023, doi: 10.1109/JIOT.2023.3235618.

[3] R. Liu, M. Li, H. Luo, Q. Liu, and A. L. Swindlehurst, "Integrated sensing and communication with reconfigurable intelligent surfaces: Opportunities, applications, and future directions," Jun. 2022, *arXiv:2206.08518v1*.

[4] Y. Liu, I. Al-Nahhal, O. A. Dobre, and F. Wang, "Deep-learning channel estimation for IRS-assisted integrated sensing and communication system," *IEEE Trans. Veh. Technol.*, vol. 72, no. 5, pp. 6181–6193, May 2023.

[5] A. M. Elbir, K. V. Mishra, M. R. B. Shankar, and S. Chatzinotas, "The rise of intelligent reflecting surfaces in integrated sensing and communications paradigms," *IEEE Netw.*, early access, Dec. 26, 2022, doi: 10.1109/MNET.128.2200446.

[6] X. Wang, Z. Fei, Z. Zheng, and J. Guo, "Joint waveform design and passive beamforming for RIS-assisted dual-functional radar-communication system," *IEEE Trans. Veh. Technol.*, vol. 70, no. 5, pp. 5131–5136, May 2021.

[7] X. Wang, Z. Fei, J. Huang, and H. Yu, "Joint waveform and discrete phase shift design for RIS-assisted integrated sensing and communication system under Cramer-Rao bound constraint," *IEEE Trans. Veh. Technol.*, vol. 71, no. 1, pp. 1004–1009, Jan. 2022.

[8] Z. Shao, X. Yuan, W. Zhang, and M. Di Renzo, "Joint localization and information transfer for RIS aided full-duplex systems," in *Proc. IEEE Global Commun. Conf. (GLOBECOM)*, Dec. 2022, pp. 3253–3258.

[9] K. Keykhosravi, G. Seco-Granados, G. C. Alexandropoulos, and H. Wymeersch, "RIS-enabled self-localization: Leveraging controllable reflections with zero access points," in *Proc. IEEE Int. Conf. Commun. (ICC)*, Jun. 2022, pp. 2852–2857.

[10] B. R. Marks and G. P. Wright, "A general inner approximation algorithm for nonconvex mathematical programs," *Oper. Res.*, vol. 26, no. 4, pp. 681–683, Jul./Aug. 1978.

[11] A. A. Nasir, H. D. Tuan, T. Q. Duong, H. V. Poor, and L. Hanzo, "Hybrid beamforming for multi-user millimeter-wave networks," *IEEE Trans. Veh. Technol.*, vol. 69, no. 3, pp. 2943–2956, Mar. 2020.

[12] H. V. Nguyen et al., "Joint power control and user association for NOMA-based full-duplex systems," *IEEE Trans. Commun.*, vol. 67, no. 11, pp. 8037–8055, Nov. 2019.

[13] A. Beck, A. Ben-Tal, and L. Tetruashvili, "A sequential parametric convex approximation method with applications to nonconvex truss topology design problems," *J. Global Optim.*, vol. 47, no. 1, pp. 29–51, May 2010.

[14] Q. Wu and R. Zhang, "Intelligent reflecting surface enhanced wireless network via joint active and passive beamforming," *IEEE Trans. Veh. Technol.*, vol. 18, no. 11, pp. 5394–5409, Nov. 2019.

[15] R. Liu, M. Li, Y. Liu, Q. Wu, and Q. Liu, "Joint transmit waveform and passive beamforming design for RIS-aided DFRC systems," *IEEE J. Sel. Topics Signal Process.*, vol. 16, no. 5, pp. 995–1010, Aug. 2022.

[16] H. Luo, R. Liu, M. Li, Y. Liu, and Q. Liu, "Joint beamforming design for RIS-assisted integrated sensing and communication systems," *IEEE Trans. Veh. Technol.*, vol. 71, no. 12, pp. 13393–13397, Dec. 2022.